Development of a New Hot Box Apparatus to Measure Building Enclosure Thermal Performance

C.J. Schumacher **D.G. Ober, PE**

J.F. Straube, PhD, PEng **A.P. Grin, PEng**
Associate Member ASHRAE

ABSTRACT

R-value is an effective, well established, and widely accepted metric for describing the thermal performance of building insulation materials but it is an incomplete metric for describing the thermal performance of building enclosure assemblies. In practice, many building designers have directly applied insulation R-value to the thermal performance of building enclosure assemblies; however, with the proliferation of new materials and enclosure systems, this simplification increasingly results in poor predictions of performance. More accurate predictions have become increasingly important as stricter energy codes and the use of compliance computer modeling have proliferated.

The thermal performance of any building enclosure assembly is highly dependent on the amount of insulation installed; however it can also be heavily influenced by a number of other factors such as air leakage, thermal bridging, operating conditions, moisture content, and installation defects. These factors are not properly or completely captured when insulation R-value is used as the sole metric for assembly thermal performance. A consortium of insulation manufacturers, representing all types of insulating materials and all regions of North America, undertook a series of research projects to examine these issues and their impact on the prediction of the thermal performance of building enclosures.

This paper documents the development of the primary apparatus used in the research: a new hot box designed to accurately measure the true thermal performance of modern wall assemblies. The approach is based on ASTM C1363. However, a number of improvements and performance extensions have been made to facilitate the research: a large, double-guarded meter box; systems to simulate heating and cooling climates without removing the test specimen; a closed-loop air transfer system that induces and measures air pressure differences across and movement through the assembly; a tracer gas system to measure unintentional and intentionally induced airflows; and the ability to measure with greater precision. All of these features allow quantification of wall assembly performance that is more representative of actual in-service conditions. The apparatus components, capacity, accuracy, calibration and validation are presented.

INTRODUCTION

R-value is an effective, well established, and widely accepted metric for describing the thermal performance of building insulation materials, but it is an incomplete metric for describing the thermal performance of building enclosure assemblies. In practice, building designers often directly apply R-value to the thermal performance of building enclosures. This practice has recently come into question as energy-cost and security issues have generated demand for building enclosures that exhibit higher levels of thermal performance. The market has responded with innovative insulation products and novel building enclosure systems such as various types of spray foam and spray-applied fibrous insulations, exterior insulated sheathing, structural insulated panel systems (SIPS), insulated concrete forms (ICF), radiant barrier systems (RBS), etc.

Because contemporary insulation materials and systems control heat flow in different, new, and non-traditional ways,

C.J. Schumacher *is a founding principal and* ***A.P. Grin*** *is a research engineer at Building Science Consulting Inc., Waterloo, Ontario, Canada.* ***D.G. Ober*** *is founding principal of Ober Engineering & Consulting LLC, Charlotte, NC.* ***J.F. Straube*** *is a professor in the Department of Civil Engineering and the School of Architecture at the University of Waterloo, Waterloo, Ontario, Canada.*

they are more or less sensitive to thermal bridging, workmanship (i.e., quality of installation), internal convection, and through convection (i.e., infiltration, exfiltration, wind washing and re-entrant looping). The impact of such "anomalies and "defects" is not captured in the R-value metric. Furthermore, the discrepancy between the actual heat flow and that predicted by combining R-values increases as the absolute temperature, the temperature difference, and the net resistance to heat flow increase. These realizations have generated a growing interest in the development of a new metric for the thermal performance of building enclosures.

NEED FOR A NEW THERMAL METRIC

To improve upon the simple addition of material R-values, a new thermal metric must address the factors known to have a significant influence on heat flow. These factors can be grouped into five categories:

1. Thermal bridging
2. Changes in material properties (e.g., with temperature or time)
3. Airflow in and through building enclosures
4. Thermal mass (including phase changes)
5. Hygric storage (and the associated latent effects and conductivity changes)

This research paper addresses only the first three categories directly.

Thermal Bridging

Thermal bridging has been, and continues to be, extensively studied. Oak Ridge National Laboratory in particular has undertaken numerous measurements and simulations of full-scale walls and collated the results in a series of papers (Christian and Kosny 1995). They proposed several definitions for assembly R-value: center-of-cavity R-value, clear-wall R-value and whole-wall R-value. The most widely adopted of these, clear-wall R-value, accounts for thermal bridging through regular, necessary framing members (e.g., studs, girts, clips) in a clear section of wall that is free of penetrations (e.g., windows, doors, vents) and intersections (e.g., with roofs, foundations, other walls) Clear-wall R-value is used in some codes and standards (e.g., ASHRAE 90.1) to define the thermal performance of building enclosures. The development and adoption of clear-wall R-value can be viewed as evidence of the industry's interest in and willingness to accept an evolution of metrics for the thermal performance of building enclosures.

Bombino and Burnett (1999) used a steady-state 2D heat flow software package and the clear-wall R-value concept to emphasize the impact of thermal bridging through steel studs and demonstrate the benefit of continuous exterior insulation. Codes have evolved to acknowledge the impact of thermal bridging; many now provide different prescriptive requirements for installed R-values in walls that employ continuous exterior insulation.

Thermal bridging problems can be made more complex by air leakage and moisture issues. Many complex thermal bridging problems can now be addressed using sophisticated, commercially-available software for predicting steady-state 2D and 3D heat flow. These computer programs cannot predict air leakage effects, thermal expansion/contraction, or moisture effects. A physical test facility is required to simulate, study, and quantify these effects in order to fully assess the impact of thermal bridging on building performance.

Changes in Material Properties

It is well accepted that a material's thermal properties can change as a function of temperature, time, moisture content, etc.

The temperature dependency of material thermal properties can have significant practical implications. Figure 1 shows the measured conductivity versus temperature for a range of materials employed in this research project. Over the temperature range that is relevant to buildings, most insulation materials exhibit a near linear increase in apparent conductivity. This is expected and largely predictable because of the role of gas conductivity and radiation. However, some refrigerant-blown foam insulation materials have been shown to exhibit dramatic and non-linear relationships between temperature and apparent conductivity (Graham 2010, Schumacher 2013), as is the case for the polyisocyanurate insulation (shown in Figure 1) that was used for the thermal break in the wall specimen cartridge.

The US Federal Trade Commission produced a significant regulation in 1979 that has profoundly impacted the reporting of insulation thermal properties in the United States and Canada. The regulations were developed to promote the comparison of insulation materials under similar conditions. The FTC R-value rule (FTC 1979) requires testing to be conducted at a mean temperature of 75°F (24°C), although it does not specify a temperature difference or an orientation for the samples. However, ASTM C1058-03 *Standard Practice for Selecting Temperatures for Evaluating and Reporting Thermal Properties of Thermal Insulation*, which is referenced by the rule, provides only one set of test temperatures with a mean of 75°F (24°C): a hot side of 100°F ± 9°F (38°C ± 5°C) and a cold side of 50°F ± 9°F (10°C ± 5°C). This is not the only set of temperatures that are allowed, but it is by far the most commonly chosen by manufacturers for testing and reporting R-values. It seems appropriate to conduct material R-value tests over a wider range of temperatures that might reflect realistic building applications. For example, insulation for a wall assembly in a cold climate might be tested with –10°F (–23°C) on the cold side and 72°F (22°C) on the warm side. Alternatively, hot-climate roof insulation could be tested at a warm side of 140°F (60°C) and a cold side of 75°F (24°C).

Realistic temperatures should also be employed in testing the thermal performance of building enclosures. When build-

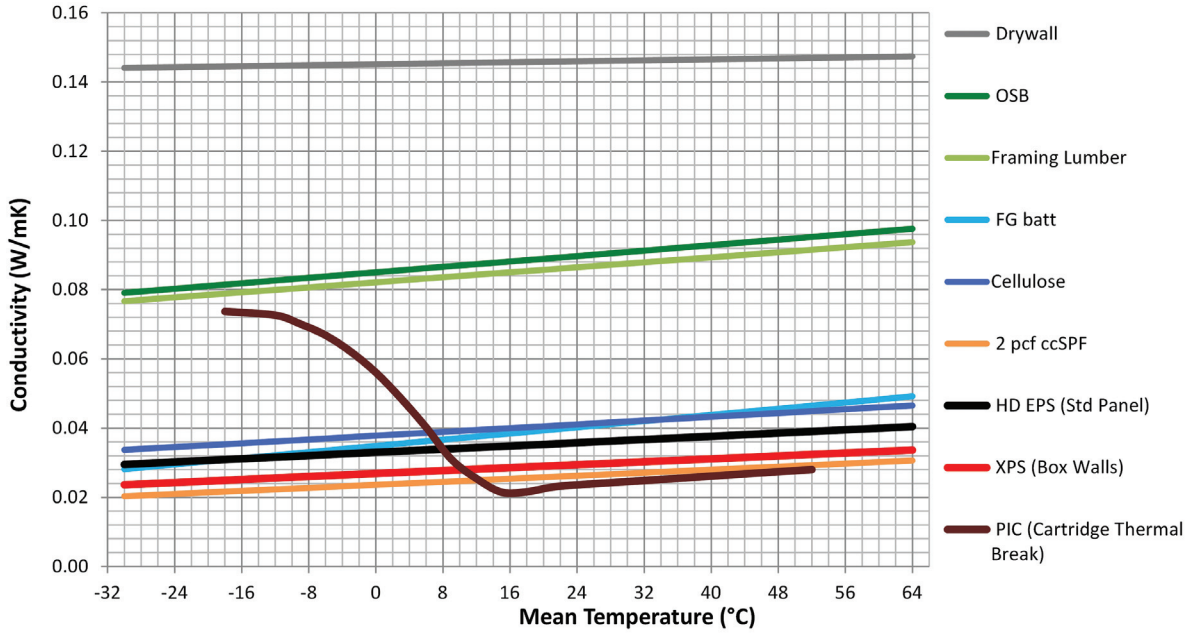

Figure 1 *Measured conductivity of selected materials used in the construction of the new hot box and in test wall specimens.*

ing enclosures are subjected to realistic temperature changes, materials expand and contract, gaps and paths open and close, and the thermal performance of the assembly changes. These effects are not easily predicted; hot box testing is often needed to assess their relevance to any comprehensive metric of assembly thermal performance.

The performances of some insulation materials also change with time. For example, some closed-cell foam insulation materials are of particular interest. ASTM C1303-07 *Standard Test Method for Predicting Long-Term Thermal Resistance of Closed-Cell Foam Insulation* (the LTTR method), was developed specifically to address gas replacement and provide an estimate of the long-term thermal performance of rigid foam insulations that use blowing agents.

Airflow in and through Building Enclosures

It has long been recognized that the control of airflow is a crucial and intrinsic part of heat and moisture control in modern building enclosures (Wilson 1963, Garden 1965). Air *can carry* heat with it and hence convection is one of the primary modes of heat transfer. Figure 2 shows four different airflow paths that influence the thermal performance of building enclosures.

Insulation material R-values do not account for any airflow through the material as a perfect air barrier is assumed somewhere in the assembly. For the purposes of building energy modeling, designers simply add the heat associated with predicted air leakage (i.e., flow path 1) to the predicted building enclosure heat flow (i.e., resulting from conduction). However, this additive approach may not properly account for the impact of air leakage. For example, Yarborough and

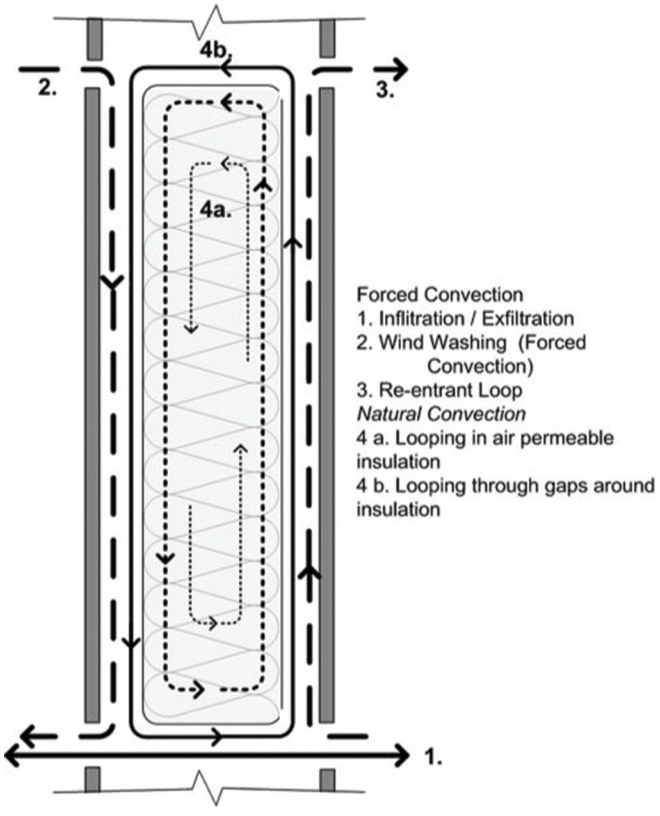

Figure 2 *Common convective airflow paths in and through enclosures.*

Graves (2006) conducted a bench top study of heat flow through air permeable insulation with imposed airflow using a modified ASTM C518 test approach. They found that the simple addition of conductive and air leakage heat flows is not sufficient to predict the measured thermal performance. This is expected because the temperature within air permeable insulation materials will vary as air flows vary through them, disturbing heat flow patterns. Airflow through diffuse and tortuous paths will result in long contact time, resulting in some heat recovery.

Lecompte (1991) conducted an extensive hot box study of the impact of convective loops (i.e., flow path 2 or 3) through small but realistic gaps between air impermeable board insulation and its substrate (i.e., continuous exterior insulation over sheathing). He measured a 30% increase in heat flow for a 1/4 in. (6 mm) gap and a doubling of heat flow for a 3/8 in. (9.5 mm) gap when considering an approximately R-10 assembly.

The impact of wind washing on thermal performance (i.e., flow path 2) has been studied in Scandinavia. Finnish research (Uvloskk 1996) demonstrated that heat loss due to wind washing in a test hut increased by 10% to 30% depending on wind speed.

Insulation products are not always installed as intended by their manufacturers or in a manner similar to how the R-value is tested. If the insulation is improperly installed or gaps form because of shrinkage or settling, flow paths can be formed. Brown et al. (1993) conducted a hot box study to assess the impact of gaps that can occur in the corners of stud spaces when batts are poorly fitted (i.e., flow paths 4a and 4b). For large gaps and large temperature differences, reductions in thermal performance of 25% to 33% were measured. Trethowen (1991) conducted a hot box study of natural convection looping around air impermeable insulation installed in a cavity (i.e., flow path 4b). In his experiment a 5/8 in. (15 mm) cavity was provided on both sides of an air impermeable e xpanded polystyrene (EPS) board insulation installed in a wood stud wall. A variable width of gap at the top and bottom of the stud space was used to investigate workmanship effects. With a gap of 1/8 in. at the top and bottom, heat flow was almost twice that of the sealed gap condition (a 50% reduction in thermal performance).

Previous full-scale physical (i.e., hot box) tests have focused on airflow paths 2, 3, and 4. Little physical testing has been conducted to assess the impact of flow paths that have air moving from one side of the wall to the other. For example, flow paths that combine 1, 2, and 3 are complex and increase the contact time and thus the potential impact on heat flow. Chebil et al. (2003) did investigate these impacts using a computer model and showed significant 8% to 15% changes in heat flow for reasonable ranges in air leakage, depending on flow path. The only comprehensive tests made of airflow through enclosure walls in a hot box were conducted by Jones, et al. (1995). They undertook the hot box measurements of 40 different assemblies with and without air leakage. The base wall was a traditional nominal R-12 2 × 4 wall with R-2.5 foam sheathing. The air leakage of the walls covered a wide range from as little as 0.3 l s/m^2 at 75 Pa to over 1.2 l s/m^2 at 75 Pa. Jones et al showed that: "Test results for the wall assemblies reveal that airflow rates as low as 0.2 L s/m^2 can produce a 46% increase in apparent thermal conductance". The influence of wind washing, although not studied in detail due to equipment limitations, was projected to reduce the thermal resistance by 18%. These percentages would be much higher for high-R walls.

NEED FOR A NEW HOT BOX

Physical measurement will be required for the development of metrics that more accurately capture the thermal performance of new building materials and systems. Laboratory testing is preferred because it permits the control necessary to isolate the influence of various parameters. However, few conventional hot boxes have ability to control important variables (e,g., temperature, air pressure, humidity) either simultaneously or within the range of interest. A new hot box apparatus is needed for this work.

DESIGN REQUIREMENTS FOR NEW HOT BOX

A new hot box apparatus was designed, constructed and commissioned to address the needs outlined above. Table 1 summarizes the design requirements that were established.

Table 1. Design Requirements for New Hot Box Apparatus

Consideration	Requirement	Motivation
Wall Area	100 square ft (9.3 m^2)	Sufficiently large to accept full-scale test wall specimens. Also to maximize signal to noise ratio.
Wall Thickness	2 to 16 in. (51 to 406 mm)	Accommodate new technologies from VIP to double stud walls.
Temperature Range	–4°F to +140°F (–20°C to +60°C)	Reproduce conditions that represent 10% of hours in cold climates through to 10% of hours on solar heated surfaces.
R-value Range	R15 to R60 (RSI-2.6 to 10.6)	Accommodate assemblies that are typical of those constructed now through to those that may be constructed in the foreseeable future.
Air Leakage Pressure Difference	±20 Pa	To reproduce conditions experienced by mid-rise buildings for 10% of the year.
Air Leakage Flow Rate	0.4 to 0.04 cfm/ square ft. at 75 Pa	Accommodate assemblies that are typical of those constructed now through to those that may be constructed in the foreseeable future.

Several other capabilities were considered for future testing: the ability to assess moisture effects (both material conductivity and latent effects) and the ability to assess dynamic effects (including thermal mass and phase change materials).

FEATURES OF THE NEW HOT BOX

In general, the new hot box apparatus has been designed and constructed in accordance with ASTM C1363, *Standard Test Method for Thermal Performance of Building Materials and Envelope Assemblies by Means of a Hot Box Apparatus*. ASTM C1363 recognizes two configurations for hot boxes: guarded and calibrated. Figure 3 provides schematics of a conventional guarded hot box, a conventional calibrated hot box, and the new hot box. In all three apparatuses the test wall specimen is installed between a meter box and a climate box. The conventional guarded hot box and the new hot box include a third box, the guard box that seeks to eliminate the temperature difference across the walls, floor, and roof of the meter box.

The new hot box features a number of improvements beyond conventional ASTM C1363 hot boxes:

- A double guard (insulated guard box plus liquid guard loop) to improve control over the temperature differential across the meter box walls and minimize uncertainties,
- Equipment to control and measure both heating and cooling of the meter box,
- An air transfer system to induce infiltration/exfiltration,
- A tracer gas system to measure air exchange over all tests (not only those run with intentionally induced air pressure differences),
- A deeper meter box to permit the testing of wall-wall and wall-floor intersections at close to full scale,
- Draw-through fans to create more realistic airflow over the inside surface of the wall specimen, and
- A modified specimen frame or "cartridge" to control flow of heat and mass at the perimeter of the metered area of the test wall specimen.

METER BOX

The meter box has a depth of 1.5 m (5 ft) to permit testing of wall-wall and wall-floor intersections at full scale. This is significantly deeper than conventional hot boxes which are usually designed to minimize depth and meter box wall area in an effort to minimize heat loss across the meter box walls. The new hot box design uses a double guard and meter box wall insulation to offset the additional wall area associated with the increased depth of the box.

Construction

All three of the hot box boxes are constructed using custom assembled structural insulated panels comprising 11 mm (7/16 in.) good, one-side plywood adhered to either side of a solid layer of 100 mm (4 in) extruded polystyrene (XPS) insulation to create a stiff, strong, airtight wall with an unbridged, continuous thermal resistance of more than RSI-3.7 (R21). These SIPs are attached to the inside of a steel exoskeleton using fasteners that only penetrate the outer layer of plywood. The meter box walls are insulated with an additional RSI-1.76 (R10) of foil-faced polyisocyanurate insulation. The foil acts as an isothermal surface to which to fasten temperature sensors, and as a low-emissivity surface that ensures a uniform radiant exposure behind the insulated air baffles.

Air Circulation and Measurement

The insulated baffles are used to form consistent vertical airflow patterns over the interior faces of the test wall specimen to ensure predictable and uniform heat transfer coefficients. The baffles consist of RSI-0.88 (R5) insulation boards with a low-emissivity foil skin facing the inside of the meter box and a painted plastic skin facing the wall specimen. The low-emissivity foil skin and the insulation ensure that the baffle is at a constant temperature close to that of the air that is travelling across the face of the test wall specimen. The painted plastic skin ensures that the surface of the test wall specimen radiates to the baffle as a real wall would to its surrounding environment. Calibrated precision thermistors (±0.1°C) are used to measure temperatures at 24 points on the baffle surface, 24 corresponding points in the air stream, and 24–36 points on the interior surface of the wall test specimen.

Airflow in the baffle space is induced by a set of DC axial circulation fans at the top or the bottom of the baffle. The fan speed can be adjusted to draw the air through the baffle space at velocities representative of natural convection in real-world conditions, typically 0.3 m/s (1 fps). The lower fans are used to draw air in and down the wall during cold climate tests while the upper fans are used to draw air in and up the wall during hot climate tests. The use of draw-through fans (rather than blow-through) ensures that velocities over the test wall specimen are uniform and the flow is not turbulent. Uniformity of the flow velocity profile over the specimen was confirmed via hot wire anemometer traverses. The voltage and current to the circulation fans are measured across precision (±0.01%) resistors so that the power added to the meter box may be calculated.

Heating System and Energy Measurement

The temperature in the meter box is controlled by electric heat and hydronic cooling. Two heating arrays, each consisting of 48 heaters and 8 mixing fans, are installed in the upper and lower portions of the mixing part of the meter box as seen in Figure 4. The size, number, and distribution of the heaters and fans ensure that the temperature is relatively uniform throughout the meter box. The heaters and fans are divided into four separately measured banks. The voltage drop across each bank is measured, using the hot box monitoring and control system (MCS), across a voltage divider comprising eight 1 Mohm ±0.1% resistors installed in paral-

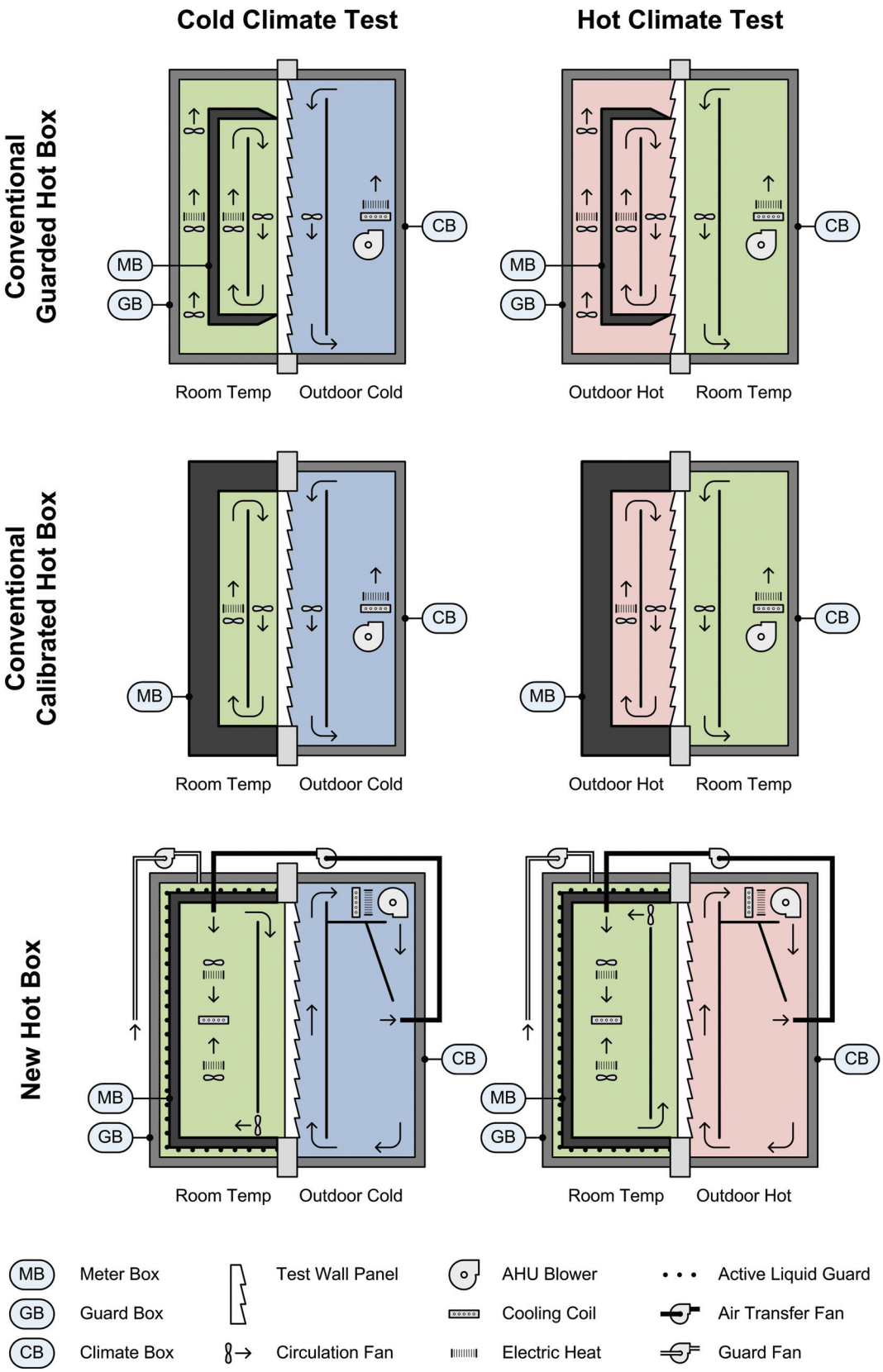

Figure 3 *Schematics of conventional guarded hot box, conventional calibrated hot box, and the new hot box apparatus developed as a result of this research.*

Figure 4 *Upper and lower heating arrays and cooling coil mounted on a movable rack in the meter box.*

lel with the resistance heaters. The monitoring and control system (MCS) also measures the current in each bank as the voltage drop across 1 ohm ±0.01% 7 W resistors with Kelvin connections. The uncertainty in power measurement is better than ±0.25% over the full range of heater output.

Cooling System and Energy Measurement

The new hot box apparatus achieves meter box cooling using a large, finned convection coil, mounted at mid-height in the air mixing part of the meter box. The large heat transfer area permits the removal of significant amounts of heat with only modest (e.g., 2°C or 3.6°F) temperature increases between the inlet and outlet of the coil. Distilled water is pumped from a chilled, constant temperature (±0.05°C) buffer tank, into the meter box, through the convection coil, and back out of the meter box. The flow rate (typically 0.5 to 1.5 lpm) is measured using a NIST traceable ±0.2% of reading flow meter and the supply and return temperatures are measured using a pair of precision thermistors (±0.1°C) and a pair of ultra-precision RTDs (±0.012ohm). These measurements can then be used to calculate the energy the cooling extracts from the meter box.

The cooling coil and the two heating arrays are mounted on a rack that can be moved forward or backward into the meter box as necessitated by the geometry of the test specimen. The overall accuracy of the cooling measurement system is estimated to be ±1.5%.

GUARD BOX

The new hot box employs a double guard: an insulated guard box surrounds the meter box and an active liquid guard loop is installed over the outside surface of the meter box as seen in the photograph of Figure 5. The guard box minimizes the influence of temperature changes in the lab and reduces spatial temperature gradients over the surface of the meter box. The liquid guard loop further reduces any spatial temperature gradients and all but eliminates any temperature difference between the inside and the outside of the meter box walls.

Figure 5 *View illustrating the double-guarded concept: a conventional guard box on the left and an active liquid guard installed on the meter box on the right.*

Construction

The guard box employs the same basic custom SIP in steel exoskeleton construction as the meter box: 11 mm (7/16 in.) good, one-side plywood skins adhered to either side of a solid layer of 100 mm (4 in) XPS insulation for a continuous thermal resistance of more than RSI-3.7 (R21).

Active Liquid Guard

The active liquid guard comprises six separate circuits of PEX piping that are attached to the outside of the meter box using aluminum heat transfer plates. The six circuits (one on each of the top, bottom, and sides, plus two on the back) are set up as secondary loops off of a primary loop that provides conditioning for the active liquid guard. Each circuit can be individually controlled with metering valves to allow the flows to be calibrated from time to time to ensure spatial uniformity of the temperature. The water flow of each loop has been designed to absorb or release the expected heat flow through the RSI-3.7 (R21) guard chamber walls (in the range of 2 to 4 W per loop) with a temperature rise of less than 0.005°C (0.009°F).

Delta T Measurement

The temperature difference or delta T across the meter box walls is measured by paired precision thermistor arrays that are applied to the inside and outside of each of the five faces of the meter box at a density of more than five sensors per square meter. In all, the temperature difference is measured at 176 locations. Using the aggregated differential temperature measurements, the hot box system controls the active liquid guard supply temperature, thereby reducing the average temperature difference across the meter box to less than 0.05°C (0.09°F). Typical average temperature difference during operation is better than 0.02°C (0.04°F).

Heating and Cooling

In the new hot box, the guard box is not conditioned using electric resistance heaters and circulation fans as is common in conventional guard boxes (which typically have no meter box cooling). Instead, the temperature in the guard box is controlled by the active liquid guard. The primary loop of the liquid guard is indirectly cooled using a plate heat exchanger. The primary loop flow rate is fixed so that the outlet temperature on the guard side of the exchanger is controlled by varying the temperature on the chiller side. This is accomplished through the use of a computer controlled three-way mixing valve. The fluid is slightly overcooled (typically 0.2°C or 0.36°F) then precisely heated to the target setpoint by a pair of pulse-controlled electric resistance band heaters.

CLIMATE BOX

The climate box has the same overall size as the guard box.

Construction

The climate box employs the same basic custom SIP-in-steel exoskeleton construction as the guard box: 11 mm (7/16 in.)

good, one-side plywood skins adhered to either side of a solid layer of 100 mm (4 in) XPS insulation for a continuous thermal resistance of more than RSI-3.7 (R21).

Air Circulation and Measurement

Insulated baffles are used to form consistent vertical airflow patterns over the exterior face of the test wall specimen and establish uniform heat transfer coefficients. The baffles use the same construction as the meter box.

Airflow in the baffle space is induced by a set of four air handling units, each with an ECM blower programmed to generate flow rates of 165, 212, 283, and 378 lps (350, 450, 600, and 800 cfm). The fan speed can be adjusted to push air through the baffle space at velocities representative of various wind speeds in real world conditions, typically 0.9 to 1.8 m/s (3 to 6 fps). The flow velocity profile can be tuned via a series of adjustable vanes located in the supply plenum at the back of the climate box. Uniformity of the flow velocity profile over the specimen was confirmed via hot wire anemometer traverses.

Heating and Cooling

The temperature in the climate box is controlled by a series of four fan coils connected to an 8 kW at –20°C (and 4.5 kW at –30°C) capacity air-cooled liquid chiller and a 3 kW hydronic heater. The oversized coils allow for a very small temperature drop across the coil during most test conditions. Reheat coils and individually-controlled tight-fitting dampers allow for individual defrost. This feature allows three fan coils to continue conditioning and circulating air while the fourth is defrosted. The reheat coils can be used for humidity control, and the low temperature drop cooling coils allow RH levels of 90% to 95% rh to be maintained over most of the temperature range. In general the chiller temperature is set to overcool and fine tuning of the temperature is accomplished using 1.5 kW of pulse-controlled electric resistance heat.

WALL SPECIMEN (SAMPLE) CARTRIDGE

Section 6.7.1 of ASTM C1363 requires the provision of a specimen frame to support the wall test specimen in position between the meter box and climate box and to insulate the perimeter of the specimen to reduce flanking heat transfer. In a conventional guarded hot box, the wall test specimen area extends beyond the perimeter of the meter box so the portion of the wall between the meter box and the climate box sees the same heat flow as the portion of the wall between the guard box and the climate box. This is an extremely effective method of minimizing flanking heat flows; however, when hollow (e.g., framed) walls are tested, it provides paths for air to flow not just between the climate box and the meter box, but also between these two boxes and the guard box.

The interaction between heat and airflow is of particular interest in this research program, hence a new specimen frame was designed to minimize flanking losses while eliminating airflow outside of the area of the wall test specimen.

Construction

The new hot box specimen frame or "cartridge" comprises alternating layers of 11 mm (7/16 in) plywood and 100 mm (4 in) XPS foam board glued up to create an exceptionally stiff sandwich panel as seen in Figure 6. Two 38 × 38 mm (nominal 2 × 2 in.) nailers are embedded in the cartridge to provide fastening support. A 100 mm (4 in) thick polyisocyanurate thermal break lines the entire rough opening of the cartridge. A 3 mm (1/8 in.) thick sacrificial MDF lining protects the polyisocyanurate insulation and facilitates air sealing between the cartridge and the test wall specimen. The finished opening of the cartridge and the size of the wall test

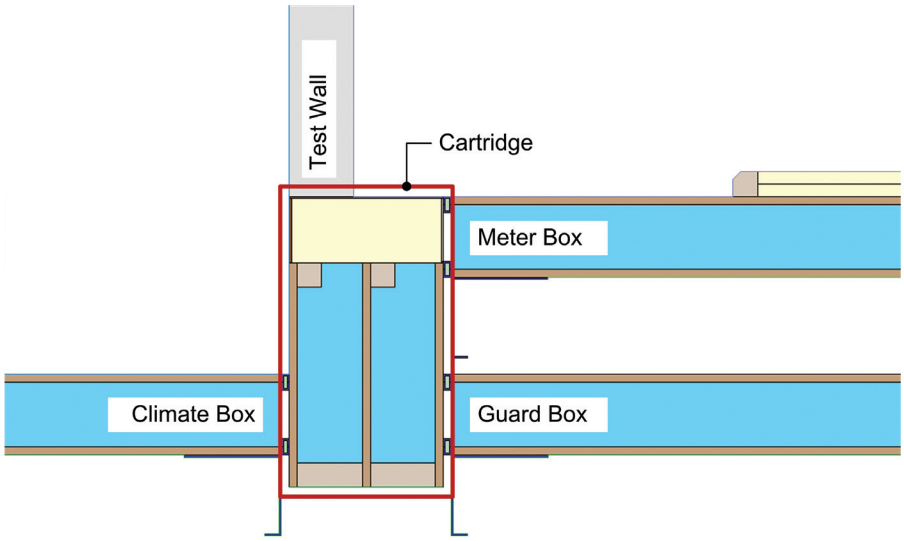

Figure 6 *Section through wall cartridge showing relationship to meter box, guard box, and climate box.*

specimen match the meter box opening: 3.66 m (12 ft) wide by 2.44 (8 ft) high.

Box-to-Box Air Sealing

Box-to-box air sealing is accomplished using two-stage joints comprising mated closed-cell foam gaskets. These air seals exist at three interfaces: between the meter box and the cartridge, between the guard box and the cartridge, and between the climate box and the cartridge. The gaskets are engaged, compressed and sealed using 20 tons of clamping force.

Sample Air Sealing

After the test specimen is installed in the cartridge, the perimeter of the test wall specimen is sealed (both inside and out) to the MDF cartridge liner using tapes and sealants as appropriate for the building materials in the test wall assembly.

PRESSURIZATION AND AIR TRANSFER SYSTEM

One of the most novel aspects of the new hot box is the air transfer system (ATS). The system, pictured in Figure 7, generates a pressure difference between the meter box and the climate box to drive airflow through available paths in the test wall specimen. The system comprises an inline fan, an inline heater, three high accuracy (±2% of reading) mass flow sensors (installed in parallel), and piping and valves to allow researchers to negatively pressurize (i.e., induce infiltration) or positively pressurize (i.e., induce exfiltration) the meter box. A guard fan is used to minimize the pressure difference between meter and guard boxes so that airflow only occurs between the meter and the climate boxes.

The system can accommodate flow rates up to 900 lpm (32 cfm) at pressures of up to 50 Pa. This imposes leakage rates of up to 100 lpm/m^2 (0.34 cfm/ft^2).

Heat transfer associated with the airflow is calculated using the measured flow rate, the heat capacity of air (at the measured pressure, temperature, and humidity) and the temperature difference between the delivered air temperature (measured using an ultra-precision RTD at ±0.012 ohm) and the air temperature in the meter box (measured using an array of precision thermistors at ±0.1°C).

TRACER GAS SYSTEM

The tracer gas system permits monitoring of the air change between the meter box and the climate box during all modes of testing. This system is vital to the research as the test wall specimens include realistic air leakage paths. Hence, airflow is induced not just by the air transfer system but also by pressure differences that naturally exist as a result of stack effect (temperature differences) and circulation fans.

The tracer gas system comprises a regulated and metered supply of 99% pure CO_2; four CO_2 sensors, one in each of the meter box, the guard box, the climate box, and the laboratory; and dilution system capable of supplying 2.5 lps (5 cfm) of dilution air at –40°C (–40°F) dew point. The meter box is

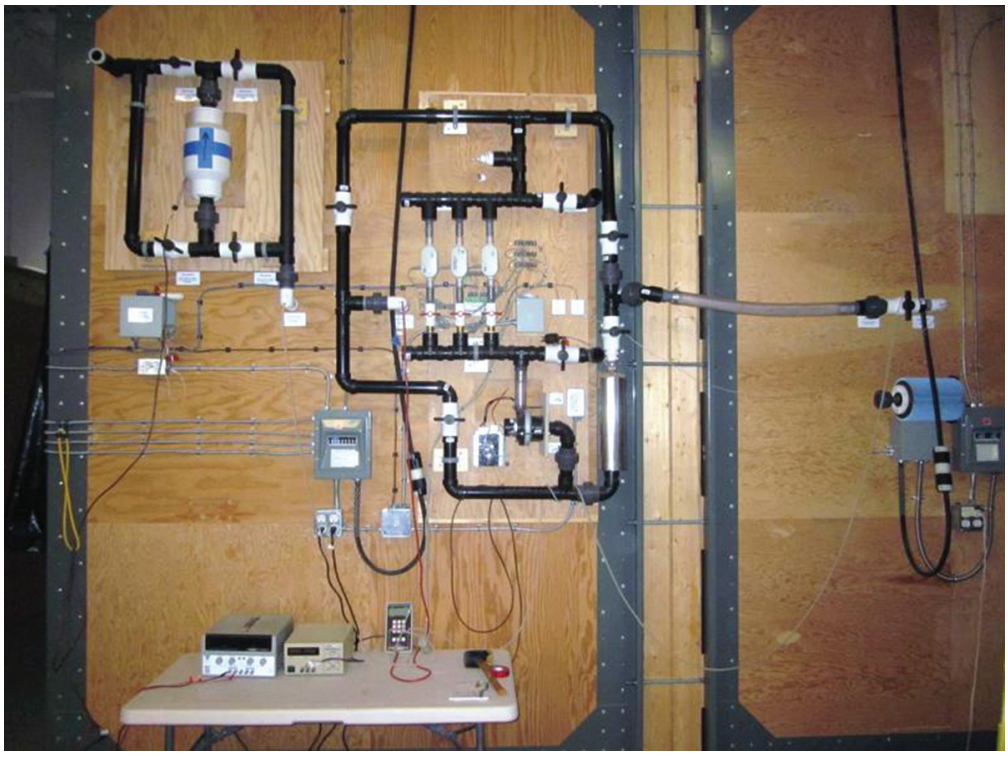

Figure 7 *Guard fan system on the left and air transfer system on the right.*

dosed to a concentration of 10,000 ppm; the air change rate between the meter box and the climate box is calculated using decay method described in *ASHRAE Handbook—Fundamentals* 2009, Chapter 16. The decay of CO_2 and correlated air transfer rate are shown in Figure 8.

TEMPERATURE MEASUREMENT (TM)

The sensors were fabricated using 10k ohm NTC precision thermistor components (Honeywell/Fenwall 192-103LET-A01) soldered to 28 AWG leads. The resulting temperature sensors are approximately the same size as the thermocouples that are typically used in hot box research.

From the manufacturer these sensors have a tolerance of ±0.2°C. The research team sought to reduce as many uncertainties as possible; hence sensors were individually calibrated over the range of temperatures in which they were to be used. The meter box guard sensors were calibrated at 16°C, 18°C, 20°C, 22°C, and 24°C while the baffle surface, air space and wall specimen sensors were calibrated at –30°C, –20°C, –10°C, 0,°C 10°C, 20°C, and 30°C.

Roughly 600 of the temperature sensors were fabricated to instrument the TM hot box and use on the test wall specimens for the first phase of research. Each sensor was assigned a unique serial number and calibrated in an aluminum calibration block set in a controlled temperature bath, a VWR 1157P, capable of maintaining the bath temperature within ±0.01°C of the setpoint. The aluminum calibration block further ensures the spatial and temporal stability of the temperature during calibration. A NIST traceable HH41 reference thermometer (±0.023°C or over the range of –20°C to 60°C) was inserted in a 100 mm (~4 in.) deep hole in the middle of the block. Sensors were calibrated in sets by inserting them in the 12 holes that circle the reference thermometer.

For each setpoint, the bath was brought to equilibrium and allowed to run for 15–20 minutes, after which five readings were taken at 1 minute intervals. For each reading, the time, the bath temperature, and the reference thermometer temperature were manually recorded. Meanwhile, the resistances of the thermistor-based temperature sensors were automatically measured and recorded using a Campbell Scientific CR1000 measurement and control system and a half-wheatstone bridge circuit with a precision (±0.01%) sense resistor. Sensor-specific calibration coefficients were determined for a third order polynomial equation. The resulting temperature sensor uncertainty is better than ±0.05°C (0.09°F).

ENERGY BALANCE

Figure 9 shows the energy balance on the meter box (MB). All heat (i.e., energy) flows are considered positive into the meter box except for the test sample heat flow which is considered positive when heat is flowing from the meter box to the climate box (CB).

Using the heat flows shown in Figure 9 results in the following energy balance:

$$Q_h + Q_c + Q_f + Q_{fl} + Q_{mw} + Q_{tas} + Q_L + Q_{ih} + Q_s = 0 \quad (1)$$

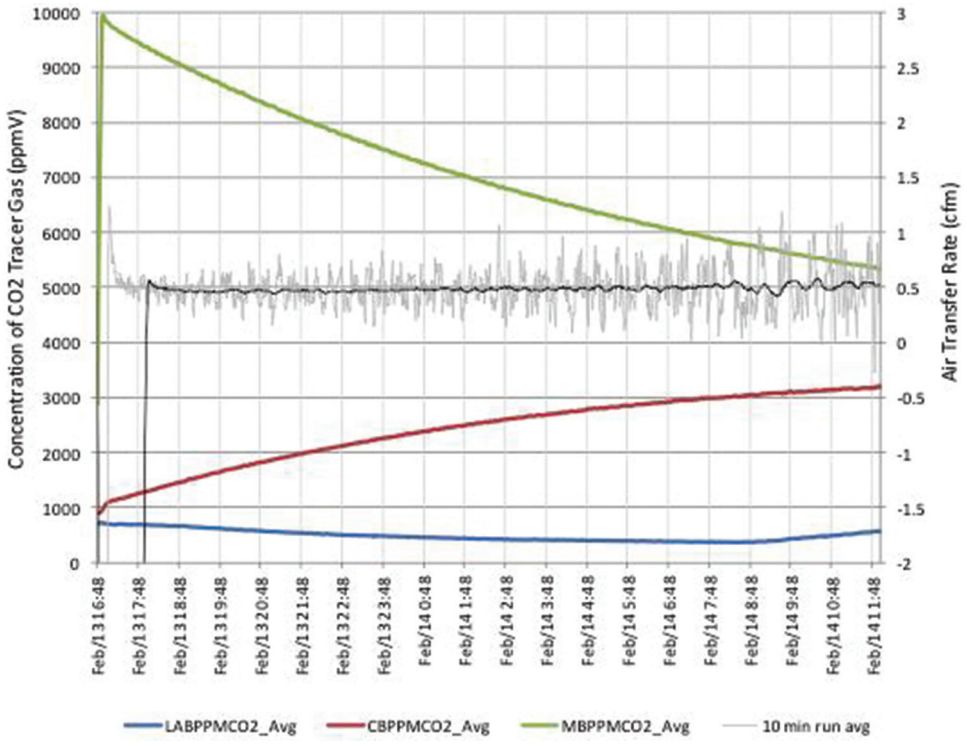

Figure 8 *CO_2 decay and air transfer rate measurement.*

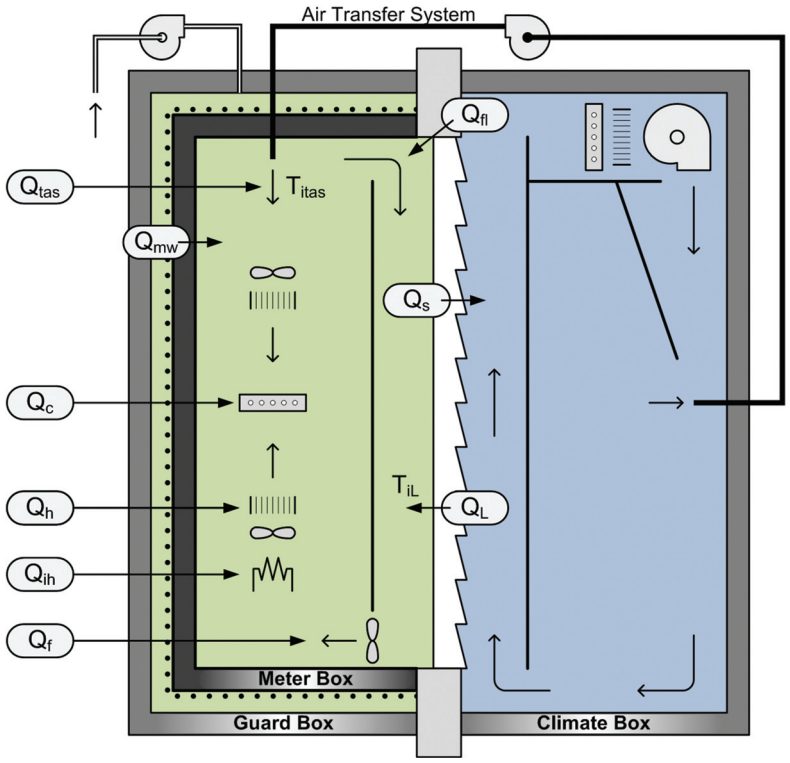

Figure 9 *Energy balance diagram for the new hot box apparatus.*

where

Q_s = heat flow through the test sample
Q_h = heat input from the electric heaters
Q_c = heat input or removal from the cooling system
Q_f = heat input from the circulation fans
Q_{fl} = flanking heat transfer through the sample cartridge and associated elements
Q_{mw} = heat exchange between the meter box and guard box through meter box walls, roof, and floor
Q_{tas} = heat flow due to air entering/exiting the meter box through the air transfer system
Q_L = heat flow due to air transfer through the sample in/out of the meter box
Q_{ih} = heat input into the independent verification heater

Temperatures and coefficients are defined as follows:

$T_{air\text{-}mb}$ = meter box air temperature
$T_{air\text{-}cb}$ = climate box air temperature
$T_{s\text{-}mb}$ = sample surface temperature on the meter box side of the sample
$T_{s\text{-}cb}$ = sample surface temperature on the climate box side of the sample
T_{itas} = air temperature at the MB/air transfer system entrance
T_{iL} = air temperature of the air at the MB/test sample interface
C_p = specific heat of air
m = mass flow rate

Temperature T_{itas} is the temperature of the air just as it enters/exits the air transfer system into the meter box. Air entering the air transfer system from the meter box represents air infiltration through the sample and is essentially at the meter box temperature. For air exfiltration air enters the meter box from the air transfer system. This needs to be included in the energy balance on the meter box whenever air flows from the air transfer system into the meter box.

Q_{tas} is calculated by

$$Q_{tas} = mc_p\,(T_{itas} - T_{air\text{-}mb}) \tag{2}$$

Q_L is calculated by

$$Q_L = mc_p\,(T_{iL} - T_{air\text{-}mb}) \tag{3}$$

For the standard hot box, $Q_{tas} = 0$, Q_L=0 and Q_{ih}=0.

For convenience Q_{tot} is defined as the heat flow that is measured during a test using the following formula

$$Q_{tot} = Q_h + Q_c + Q_f + Q_{mw} \tag{4}$$

Q_{net} is defined as needed in the sections below.

Flanking Heat Transfer Prediction

For most calibrated hot boxes Q_{fl} is determined through a series of calibration tests with samples of known thermal proper-

ties. While valid, this approach runs the potential risk of associating any other extraneous errors in measurement or design solely with Q_{fl}. Another approach that was used by one of the authors in a previous calibrated hot box design avoids this potential problem. Since in a well-designed, calibrated hot box the flanking heat flow is a conductive heat flow through materials whose material properties can be measured, it is possible to predict Q_{fl} using finite element programs and then incorporate the predicted Q_{fl} into the energy balance. Then one or more samples of known thermal properties are tested to verify the overall operation of the hot box. This approach eliminates any arbitrary calibration constants. An additional advantage of this approach is that any interactions between a test sample and the sample cartridge can be investigated prior to testing to assess the sample/cartridge interaction and that effect, if any, on Q_{fl}.

Q_{fl} is a function of the following major factors:

- Cartridge geometry (fixed)
- Material thermal properties (measured)
- Film coefficients
- Test sample thickness
- Temperature

A 2D finite element program was then used to predict Q_{fl}. Figure 10 shows the model used in the finite element program. A typical output is shown in Figure 11. The results from the numerical simulation were post processed to obtain the correct area weighting. Runs were made for several film coefficients and sample thicknesses. Table 2 and Table 3 show the variation of Q_{fl} for three levels of film coefficients and four sample thicknesses. Table 2 shows Q_{fl} in Watts per degree Kelvin, while Table 3 shows the data in total Watts. The interior film coefficient (h_{in}) was fixed at 7 W/m^2·K typical of the heat transfer coefficient on the indoor side of an assembly. The exterior film coefficient (h_{out}) was varied from 7 to 14 to 28 W/m^2·K. The panel thickness was modeled from 4 in. to 6.5 in. to cover the range of test wall specimens considered in the first phase of testing with the new hot box apparatus. There is a substantial effect on Q_{fl} for different test sample thicknesses but only a small effect due to the film coefficients.

MATERIAL PROPERTY DATA

After the hot box was assembled, the thermal properties of the cartridge materials were measured over a temperature range of –18°C to +42°C using the C518 machine.

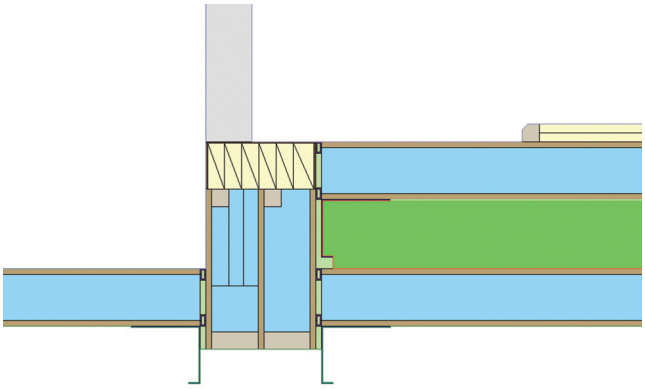

Figure 10 *Model of wall cartridge for predicting flanking using 2D finite element heat transfer program.*

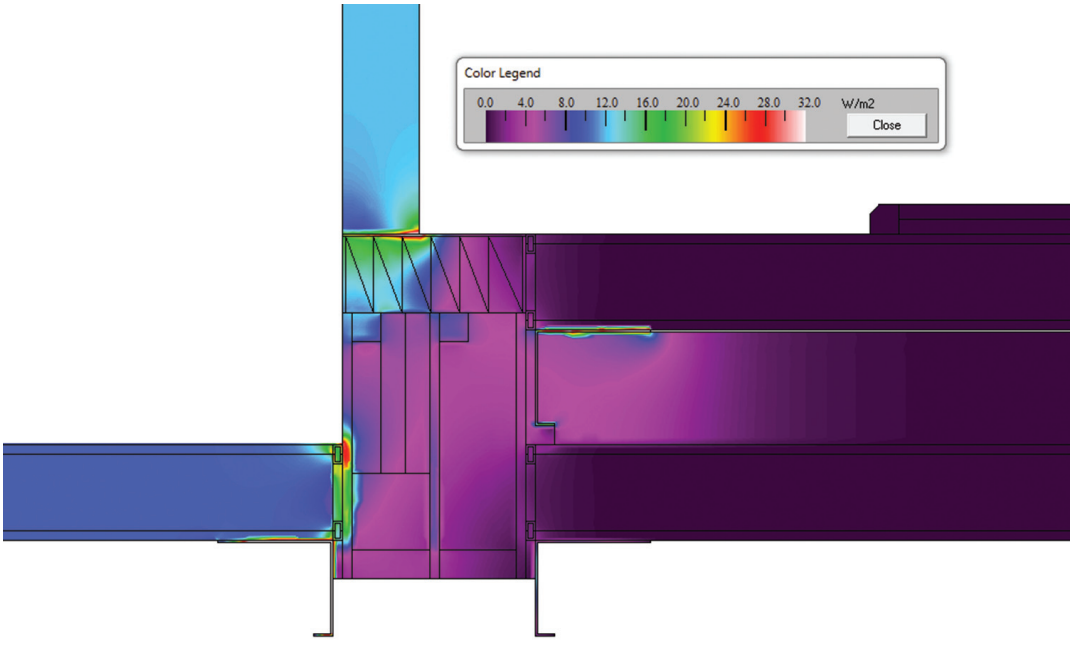

Figure 11 *Heat flux intensities predicted using 2D finite element heat transfer program.*

Table 2. Flanking Heat Flow (in W/K) Calculated from the Finite Element Program

				Climate Box Temperature				
Wall Thickness		h_{in}	h_{out}	62°C	42°C	2°C	–18°C	–28°C
(in.)	(mm)	($W/m^2 \cdot K$)	($W/m^2 \cdot K$)	Correction as Function of Air-Air delta T (W/K)				
			7	0.2816	0.2681	0.2835	0.4301	0.4756
4	101.6	7	14	0.2855	0.2717	0.2894	0.4393	0.4886
			28	0.2863	0.2740	0.2896	0.4444	0.4928
			7	0.2523	0.2425	0.2527	0.3737	0.4124
4.5	114.3	7	14	0.2558	0.2456	0.2578	0.3829	0.4213
			28	0.2573	0.2471	0.2596	0.3869	0.4261
			7	0.2303	0.2179	0.2444	0.3303	0.3556
5	127	7	14	0.2310	0.2204	0.2478	0.3364	0.3645
			28	0.2344	0.2238	0.2502	0.3416	0.3682
			7	0.1693	0.1603	0.1717	0.2454	0.2795
6.5	165.1	7	14	0.1711	0.1620	0.1737	0.2494	0.2841
			28	0.1718	0.1628	0.1747	0.2533	0.2869

Table 3. Flanking Heat Flow (in W) Calculated from the Finite Element Program

				Climate Box Temperature				
Wall Thickness		h_{in}	h_{out}	62°C	42°C	2°C	–18°C	–28°C
(in.)	(mm)	($W/m^2 \cdot K$)	($W/m^2 \cdot K$)	Correction as Function of Air-Air delta T (W/K)				
			7	11.27	5.36	–5.67	–17.21	–23.78
4	101.6	7	14	11.42	5.43	–5.79	–17.57	–24.43
			28	11.45	5.48	–5.79	–17.78	–24.64
			7	10.09	4.85	–5.05	–14.95	–20.62
4.5	114.3	7	14	10.23	4.91	–5.16	–15.32	–21.06
			28	10.29	4.94	–5.19	–15.47	–21.30
			7	9.21	4.36	–4.89	–13.21	–17.78
5	127	7	14	9.24	4.41	–4.96	–13.46	–18.22
			28	9.38	4.48	–5.00	–13.66	–18.41
			7	6.77	3.21	–3.43	–9.82	–13.97
6.5	165.1	7	14	6.84	3.24	–3.47	–9.97	–14.21
			28	6.87	3.26	–3.49	–10.13	–14.35

Thermal conductivity data was measured for the following materials and is shown in Figure 1.

- Expanded polystyrene (EPS) used for the standard samples
- Extruded polystyrene (XPS) used in the hot box walls
- Polyisocyanurate used in the cartridge thermal break
- Spruce/pine/fir (SPF) used in the cartridge thermal break
- Plywood used as an external surface for the hot box walls
- Hardboard (MBF) used as an air sealing surface for cartridge thermal break
- Steel used for the exoskeleton support structure

EPS Thermal Properties

The following equation was used to predict the thermal conductivity of the EPS for the standard sample versus mean temperature, T_m:

$$k = 0.032975 + 0.000116\ T_m \text{ (W/m K)} \quad (5)$$

XPS Thermal Properties

XPS thermal properties used in the hot box are given by:

$$k = 0.026833 + 0.0001067\ T_m \text{ (W/m K)} \quad (6)$$

Polyisocyanurate Thermal Properties

The polyisocyanurate used in the cartridge walls shows a substantial increase in thermal conductivity at temperatures below about 10°C. This is due to condensation of the blowing agent which increased the thermal conductivity. Considerable testing in using the C518 equipment was performed to characterize the thermal conductivity of this polyisocyanurate versus mean temperature. In particular, we were interested in the thermal conductivity at small temperature differences. This involved first verifying that the C518 calibration was valid for temperature differences as small as 3°C. Once this verification was complete, the polyisocyanurate was tested at each mean temperature at temperature differences of 12°C, 9°C, 6°C, and 3°C. Table 4 summarizes the thermal break conductivity measured at nineteen mean temperatures. This thermal conductivity data was then used in numerical heat transfer program to predict Q_{fl} as described above.

Other Thermal Properties

These properties are based on handbook values at 24°C since these components have a small effect on the overall thermal resistance.

SPF – k = 0.0862 (W/m K)

Plywood – k = 0.0l0913 (W/m K)

Hardboard – k = 0.1053 (W/m K)

Steel – k = 50 (W/m K)

Except for the polyisocyanurate all the materials show expected variation with mean temperature (i.e., lower thermal conductivities with lower mean temperatures).

STANDARD SAMPLE CONSTRUCTION FOR HOT BOX VERIFICATION

A nominal 12 × 8 ft standard sample was assembled, consisting of two layers of 2 in. thick 25 kg/m^3 EPS sheets. The EPS had been previously purchased and allowed to age for 6 months. The joints in each layer were staggered to minimize short circuiting through the joints and to provide structural integrity. The two layers were glued together. The exterior surfaces were then painted black to seal the sample against air leakage and to provide a high emissivity surface which simulates normal building construction emissivities. After assembly, thickness measurements were made around the perimeter of the sample. During assembly, samples of the EPS were retained for testing per C518. After assembly the finished sample was cut to the size of the opening in the sample cartridge to assure a tight fit.

The retained specimens were tested per C518 over a temperature range of –18°C to +52°C (0°F to 126°F) as discussed previously. A linear thermal conductivity versus mean temperature (T_m) curve was fit to the data.

VERIFICATION OF THE BASIC HOT BOX ENERGY BALANCE WITH NO AIR LEAKAGE

The verification sample was installed in the cartridge. Tests were run from –28°C to +62°C (–18°F to +144°F) with no air leakage. CO_2 tracer gas decay measurements confirmed that air leakage did not contribute to heat transfer.

Table 5 compares the hot box measurements on the verification sample with the assigned R-value from the C518 tests. In this table, $Q_{net} = Q_{tot} + Q_{fl}$ and Q_{std} is calculated as follows for the standard sample.

$$Q_{std} = kA(T_{out} - T_{in})/t \quad (7)$$

where

k = the standard sample thermal conductivity calculated using the C518 at the mean temperature of the hot box test

A = the sample area

t = the sample thickness

T_{out} = the surface temperature on the CB side of the sample

T_{in} = surface temperature on the MB side of the sample

Q_{std} is the expected heat flow and Q_{net} is the measured heat flow from the hot box tests. The agreement is within ±2% as shown in Table 5. Q_{fl} was calculated specifically for these tests and will vary slightly from the values shown in Table 1.

VERIFICATION OF COOLING SYSTEM ENERGY MEASUREMENTS

One of the unique features of this hot box is the capability to test under both winter and summer conditions where cooling is required for the meter box. The cooling energy measurements are generally not as accurate as the heating energy measurements. This is due to the requirement to measure cooling energy by measuring the mass flow rate of the cooling fluid and a relatively small temperature change in the fluid. To verify the accuracy of the cooling energy measurements, a test was first performed using the verification sample under cooling conditions and then adding an independent nominal 40 W electrical load in the meter box which required the same amount of cooling energy to offset the increased electrical load. Table 6 shows the energy measurement for the first test and the energy balance with the nominal 40W increased heat load. The 40W increased load, since it was an electrical load, could be measured very accurately. The cooling system has to offset this load.

As shown in the table, the Q_{net} for the baseline case is –72.0W. With added nominal 40W electrical heater the energy balance for this case is

$$Q_{net} = Q_{tot} + Q_{ih} = –109.5 \text{ W} + 36.1 \text{ W} = –73.4 \text{ W} \quad (8)$$

where Q_{ih} is the measured energy input to the added independent nominal 40W heater.

The agreement on the total energy load is 1.9%.

VERIFICATION OF AIR LEAKAGE ENERGY LOADS

To verify that energy balances are accurate when air leakage is occurring, four tests were performed for infiltration and exfiltration using two different orifice sizes. First, the standard sample was tested and the energy use measured. This was done under summer conditions. Then a 1 in. diameter hole was carefully made in the sample and tests were repeated under the same temperature conditions for air infiltration (airflow from the CB to the MB) and for air exfiltration (airflow from the MB to the CB). For the 0.25 in. hole a plate with a 0.25 in. hole in it was placed over the 1in. hole on the CB side. The 1 in. diameter tests will be discussed in detail. Table 7 shows the measurements.

The energy balance for these cases is

$$Q_h + Q_c + Q_f + Q_{fl} + Q_{mw} + Q_{tas} + Q_L + Q_{ih} + Q_{1D} = 0 \quad (9)$$

$$Q_{net} = Q_{tot} + Q_{tas} + Q_L + Q_{1D}$$

For air infiltration Q_{iL} is calculated from

$$Q_{iL} = mc_p(T_{air–cb} – T_{air–mb}) \quad (10)$$

since $T_{iL} = T_{air–cb}$. For air exfiltration $Q_{iL} = 0$ since $T_{iL} = T_{air–mb}$.

For air exfiltration Q_{tas} is calculated from

$$Q_{tas} = mc_p(T_i – T_{air–mb}) \quad (11)$$

since T_i is measured. For air infiltration $Q_{tas} = 0$ since $T_i = T_{air–mb}$.

Table 4. Thermal Conductivity Measurements for Polyisocyanurate Insulation Used as Thermal Break in Sample Cartridge

Mean Temperature T_m (°C)	Thermal Conductivity (W/mK)
–18	0.0742
–12	0.0737
–9	0.0712
–6	0.0681
–3	0.0635
0	0.0576
3	0.0502
6	0.0420
9	0.0328
12	0.0254
15	0.0215
18	0.0216
21	0.0229
24	0.0236
30	0.0245
36	0.0255
42	0.0264
52	0.0280
58	0.0290

Solid (Baseline) test: the heat flow for the baseline case is –72.0 W.

Air Infiltration

For this test air was flowing from the CB to the MB through the hole. The flow rate was 61.5 lpm. Q_{net} is calculated as follows:

$$Q_{net} = Q_{tot} + Q_{tas}$$

$$= –97.5\text{W} + 61.5 \text{ lpm} \times 1006 \text{ J/kg·K} \times 1.183 \text{ kg/m}^3 \times (42.04 – 21.90) \text{ C/ } (1000 \text{ L/m}^3 \times 60 \text{ min/s})$$

$$= 72.6 \text{ W}$$

This is 2.2% different from the baseline case.

Table 5. Comparison of Hot Box Measurements and Expected Heat Flow through Standard Verification Panel

		Units	Test Conditions				
Nominal MB Temperature		**°C**	**22**	**22**	**22**	**22**	**22**
Nominal CB Temperature		**°C**	**62**	**42**	**2**	**–18**	**–28**
CB Air *T*		°C	61.5	41.9	2.0	–17.9	–27.9
Wall Surf T_{out}		°C	60.5	41.3	2.6	–16.6	–26.1
MB Air *T*		°C	22.1	22.0	21.5	21.2	21.1
Wall Surf T_{in}		°C	24.08	23.0	20.6	19.5	19.0
Measured Heat Flow	Q_{tot}	W	–141.7	–68.5	62.8	126.6	157.5
Flanking Heat Flow	Q_{fl}	W	11.78	5.63	–5.83	–17.79	–24.55
	Q_{net}	W	–129.94	–62.87	57.01	108.83	132.99
Standard Sample Heat Flow Based on Assigned Thermal Properties							
Standard Sample Heat Flow	Q_{std}	W	–127.76	–62.14	56.67	109.28	134.20
Difference	$Q_{net} - Q_{std}$	W	–2.18	–0.73	0.34	–0.45	–1.21
% diff			1.7%	1.2%	0.6%	–0.4%	–0.9%

Table 6. Data for Verification of Cooling System Measurement

	Units	Test Conditions: Baseline	Test Conditions: Added Heater
Nominal MB Temperature	**°C**	**22**	**22**
Nominal CB Temperature	**°C**	**42**	**42**
Extra Heat Input	—	No	Yes
CB Baffle Inlet *T*	°C	42.04	42.04
	°F	107.7	107.7
MB Baffle Inlet *T*	°C	21.85	21.85
	°F	71.3	71.3
Wall Surf T_{out}	°C	41.55	41.55
	°F	106.8	106.8
Wall Surf T_{in}	°C	23.07	23.03
	°F	73.5	73.5
TASdmT	°C	NA	NA
	°F	NA	NA
Airflow	SLPM	—	—
	CFM	—	—
Q_{tot}	W	–72.0	–109.5
	btu/h	–245.6	–373.6
Q_{ih}	W	NA	36.1
	btu/h	NA	123.2
Q_{net}	W	–72.0	–73.44
	btu/h	–245.6	–250.4
Percent Difference		—	1.9%

Air Exfiltration

For this test air was flowing from the MB to the CB through the hole. The flow rate was 58.5 lpm. Q_{net} is calculated as follows:

$$Q_{net} = Q_{tot} + Q_{tas}$$

$$= -77.0\text{W} + 58.5\ \text{lpm} \times 1006\ \text{J/kg·K} \times 1.183\ \text{kg/m}^3 \times (27.5 - 21.83)\ \text{C/}\ (1000\ \text{L/m}^3 \times 60\ \text{min/s})$$

$$= 70.6\ \text{W}$$

This is 2.0% different from the baseline case.

For the 0.25" orifice test the tests are within –3.2% and –2.2% respectively of the baseline case.

SUMMARY

The thermal performance of wall assemblies in buildings is complex. The thermal performance of building enclosures is heavily influenced by a number of factors such as insulation level, air leakage, thermal bridging, operating conditions, moisture content, and installation defects. Simple R-value metrics do not capture all of these factors. It has been recognized that there is a need to develop new thermal metrics that provide better ways to characterize these factors. It was recognized that more sophisticated testing would be required to understand these factors prior to developing the new metrics.

The hot box described in this paper has been designed to meet the requirements of C1363. The hot box has the following features and capabilities.

1. Full wall sample size
2. Capability to test large thermal bridging configurations such as wall/wall, wall/floor, and wall/ceiling thermal bridges
3. Simultaneous measurement of heat flows that include air infiltration/exfiltration

Table 7. Data for Verification of Air Transfer System Measurement

		Solid Panel	1 in. Diameter Hole		0.25 in. Diameter Orifice	
	Units	**Test Conditions**				
Nominal MB Temperature	**°C**	**22**	**22**	**22**	**22**	**22**
Nominal CB Temperature	**°C**	**42**	**42**	**42**	**42**	**42**
Air Leakage Direction		none	infiltration	exfiltration	infiltration	exfiltration
CB baffle inlet *T*	°C	42.04	42.04	42.04	42.02	42.04
	°F	107.7	107.7	107.7	107.6	107.7
MB baffle inlet *T*	°C	21.85	21.90	21.83	21.93	21.85
	°F	71.3	71.4	71.3	71.5	71.3
Wall surf T_{out}	°C	41.55	41.56	41.51	41.50	41.52
	°F	106.8	106.8	106.7	106.7	106.7
Wall surf T_{in}	°C	23.07	23.10	23.05	23.15	23.05
	°F	73.5	73.6	73.5	73.7	73.5
TASdmT	°C	NA	21.60	27.50	21.20	25.00
	°F	NA	70.9	81.5	70.2	77.0
Airflow	SLPM	0.00	61.50	58.50	40.00	40.00
	CFM	0.00	2.17	2.07	1.41	1.41
Q_{tot}	W	–72.0	–97.5	–77.0	–85.2	–72.5
	btu/h	–245.6	–332.7	–262.7	–290.7	–247.4
Q_{tas}	W	NA	0	6.4	0	2.5
	btu/h	NA	0	21.9	0	8.5
Q_L	W	NA	23.9	0	15.5	0
	btu/h	NA	81.5	0	52.9	0
Q_{net}	W	–72.0	–73.6	–70.6	–69.7	–70.0
	btu/h	–245.6	–251.1	–240.8	–237.8	–238.8
Percent Difference	%	—	2.2%	–2.0%	–3.2%	–2.8%

4. Air leakage (infiltration/exfiltration) measurements as a function of outdoor air temperature that include contraction/expansion effects on specimen integrity
5. Measurements under both winter and summer outdoor temperatures without removing the sample

Future capabilities will include building assemblies that include moisture transfer and thermal mass effects.

A unique approach was used in formulating the energy balance on the meter box. For this facility the flanking heat flow was predicted using a finite element heat transfer program. The inputs for analysis included measured thermal property data for the materials used in the hot box construction. The other heat flows to the meter box were all measured. This approach eliminates the need to calibrate the box which can mask other errors in design or measurement. In order to verify the accuracy of this approach, a standard sample of known thermal properties was constructed to verify. Verification of three features of the hot box have been performed. Energy balances were verified for the following conditions:

1. Verification of heat flows under standard hot box conditions (no air leakage) that verified that the flanking heat flows were accurately modeled under both summer and winter conditions
2. Verification of the accuracy of the cooling measurements using an independent heat source in the meter box
3. Verification of the accuracy of the energy balances for both exfiltration/infiltration air leakages using two sizes of orifices.

The verification exercises suggest that the accuracy of the hot box is better than ±5% for measurements under both summer and winter conditions including infiltration/exfiltration air leakages.

REFERENCES

ASHRAE. 2009. *ASHRAE Handbook—Fundamentals*. Atlanta: American Society of Heating Refrigeration and Air Conditioning Engineers, Inc.

ASTM C518-04. 2004. *Standard Test Method for Steady-State Thermal Transmission Properties by Means of the Heat Flow Meter Apparatus*.

ASTM C1058-03. 2003. *Standard Practice for Selecting Temperatures for Evaluating and Reporting Thermal Properties of Thermal Insulation*.

ASTM C1303-07. 2007. ASTM C1303-07 *Standard Test Method for Predicting Long-Term Thermal Resistance of Closed-Cell Foam Insulation*.

ASTM C1363-05. 2005. *Standard Test Method for Thermal Performance of Building Materials and Envelope Assemblies by Means of a Hot Box Apparatus*.

Bombino, R. and Burnett, E.F.P. 1999. Design Issues with Steel-stud-framed Wall Systems, PHRC Research Series: Report No. 58: 44, The Pennsylvania Housing Research Center, University Park.

Brown, W.C., Bomberg, M.T., Ullet, J.M. and Rasmussen, J. Measured Thermal Resistance of Frame Walls with Defects in the Installation of Mineral Fibre Insulation, *J. of Thermal Insulation and Building Envelopes*, Vol 16, April 1993: 318-339.

Chebil, S., Galanis, N. and Zmeureanu, R. 2003. Computer Simulation of Thermal Impact of Air Infiltration Through Multi-layered Exterior Walls. Proc. of Eight International IBPSa Conference, Eindhoven, Netherlands, August 2003: 155-162.

Christian, J.E., and J. Kosny. 1995. Toward a national opaque wall rating label. *Thermal Performance of the Exterior Envelopes of Buildings* VI. Atlanta: American Society of Heating, Refrigerating and Air-Conditioning Engineers, Inc.

FTC. 1979. Home Insulation Rule, 16 CFR Part 460. Washington, DC: Federal Trade Commission.

Garden, G.K., 1965. Control of Air Leakage is Important. *Canadian Building Digest* 72, National Research Council of Canada, Ottawa, Canada.

Graham, M.S. 2010. R-value Concerns. Professional Roofing, May 2010: 24p. National Roofing Contractors Association, Rosemont, IL.

Jones, D.C., Ober, D.G. and Goodrow, J.T. 1995. Thermal Performance Characterization of Residential Wall Systems Using a Calibrated Hot Box with Airflow Induced by Differential Pressures, Airflow Performance of Building Envelopes, Components and Systems, ASTM STP 1255: 197-228, American Society for Testing and Materials, Philadelphia, PA.

Lecompte, J., 1990. Influence of Natural Convection in an Insulated Cavity on the Thermal Performance of a Wall, Insulation Materials, Testing and Applications, ASTM STP1030: 397-420. D.L. McElry and J.F. Kimpflen, Eds., Amercian Society for Tesitng and Materials, Philadelphia, PA.

Schumacher, C.J., 2013. Temperature Dependence of R-values in Polyisocyanurate Roof Insulation, Building Science Info Sheet 502, BuildingScience.com, Somerville, MA.

Trethowen, H.A., 1991. Sensitivity of Insulated Wall and Ceiling Cavities to Workmanship, *J. of Thermal Insul.*, Vol 15, October 1991.

Uvslokk, S., 1996. The Importance of Wind Barriers for Insulated Timber Frame Constructions, *J. Thermal Insul. & Building Envelopes*, Vol. 20, July 1996.

Wilson, A.G., 1963. Air Leakage in Buildings, *Canadian Building Digest* 23, National Research Council of Canada, Ottawa, Canada.

Yarbrough, D.W., Graves, R.S., 2006. The Effect of Airflow on Measured Heat Transport Through Wall Cavity Insulation, Proceedings at 2006 ASTM Symposium on Heat, Air, and Moisture Transport in Buildings, Toronto, Canada.